varactors needed for the branch type duplexer is not as great as the above would indicate. Because of the greater inherent isolation of the balanced duplexer, only one stage of isolation would be needed where the branched duplexer requires two stages. Thus the advantage in the number of varactors is two-to-one not four-to-one between the two configurations.

CONCLUSIONS

Varactor semiconductor duplexers and limiters can be designed in a consistent manner to handle a specified amount of power. With use of varactors with a given Q and erg rating, the limitation in peak power that a duplexer or limiter can be designed to handle is limited only by the resulting low-power insertion loss. The two

way insertion loss of the duplexer is dependent on the Q^2 of the varactor used. This insertion loss can be distributed within the wide limits between the transmit and receive cycles. From the standpoint of the design of the varactor duplexer, it is best to place most of the insertion loss in the receive state. The insertion loss on the transmit cycle determines the power handling capability of the duplexer.

Varactor solid-state duplexers differ from TR or ferrite duplexers in that there is essentially no spike leakage. The flat leakage energy that reaches the mixer diodes during transmitting is much less severe than the same ergs of spike leakage; therefore, the energy per pulse reaching the mixer diode may be safely higher than if a TR device is used.

Interdigital Band-Pass Filters*

GEORGE L. MATTHAEI†, MEMBER, IRE

Summary—The design of band-pass filters using interdigital arrays of resonator line elements between parallel ground planes is discussed. Two approximate design procedures are described, both of which permit design directly from lumped element, low-pass, prototype filters. Both design procedures will work for either narrow- or wide-band filters, but one procedure gives more practical dimensions for filters having wide bandwidths (such as an octave), while the other gives more practical dimensions for filters having narrow or moderate bandwidth. The resulting filters are very compact, have relatively noncritical manufacturing tolerances, and strong stop bands with the second pass band centered at three times the center frequency of the first pass band. The dimensions and measured performance curves are presented for a 10 per cent bandwidth design and an octave bandwidth design.

I. INTRODUCTION

INTERDIGITAL line structures have in the past been regarded as of interest mainly for use as slow-wave structures. (See, for example, the work of Butcher,[1] Fletcher,[2] and Leblond and Mourier.[3]) How-

ever, a recent study[4] has shown that interdigital line structures also have very interesting band-pass filter properties. In that study, various image-impedance and image-propagation phase properties of interdigital line structures were determined, and the results were verified by experimental tests on an interdigital line structure. In this present discussion a different point of view is utilized to obtain approximate design equations for interdigital filters with specified pass-band and cutoff characteristics.

Fig. 1 shows one type of interdigital filter to be discussed. The structure, as shown, consists of TEM-mode strip-line resonators between parallel ground planes. Each resonator element is a quarter-wavelength long at the midband frequency and is short-circuited at one end and open-circuited at the other end. Coupling is achieved by way of the fields fringing between adjacent resonator elements. The design equations to be presented for this case (for which the terminating lines are short-circuited) give filter structural dimensions that will be most practical when the filter is of narrow or moderate bandwidth (say, 30 per cent bandwidth or less). In this structure each line element serves as a resonator, except for the input and output line elements which have an impedance-matching function.

¹ P. N. Butcher, "The coupling impedance of tape structures," *Proc. IEE (London)*, B, vol. 104, pp. 177–187; March, 1957.
² R. C. Fletcher, "A broad-band interdigital circuit for use in traveling-wave-type amplifiers," PROC. IRE, vol. 40, pp. 951–958; August, 1952.
³ A. Leblond and G. Mourier, "Etudes lignes a barreaux a structure periodique pour tubes électroniques UHF," *Annales de Radioélectricité*, pt. 1, April, 1954; pt. 2, October, 1955.

⁴ J. T. Bolljahn and G. L. Matthaei, "A study of the phase and filter properties of arrays of parallel conductors between ground planes," PROC. IRE, vol. 50, pp. 299–311; March, 1962.

Fig. 2 shows another type of interdigital filter, it differs from the filter in Fig. 1 in that the terminating lines are open-circuited instead of short-circuited. The design equations to be given for this type of interdigital filter will give filter structural dimensions that are most practical when the filter is of moderate to wide bandwidth (say, around 30 per cent bandwidth or greater). In this case all of the line elements serve as resonators, including the open-circuited terminating line element at each end.

Interdigital band-pass filters have a number of very attractive features.

1) They are very compact.
2) The tolerances required in their manufacture are relatively relaxed as a result of the relatively large spacings between resonator elements.
3) The second pass band is centered at three times the center frequency of the first pass band, and there is no possibility of spurious responses in between. (Note that for filters with half-wavelength, parallel-coupled resonators[5],[6] even the slightest mistuning will result in narrow spurious pass bands at twice the frequency of the first pass-band center.)
4) The rates of cutoff and the strength of the stop bands are enhanced by multiple-order poles of attenuation at dc and at even multiples of the center frequency of the first pass band.
5) These filters can be fabricated in structural forms which are self-supporting so that dielectric material need not be used. Thus dielectric loss can be eliminated.

If all of the coupling effects are accounted for, the mathematics that describe the performance of interdigital filters such as those in Figs. 1 and 2 become quite unwieldy.[4] Since synthesizing a structure to have a prescribed response is a much more difficult problem than analyzing a given structure, and since an exact analysis of this structure is itself very tedious, the prospects of obtaining a usable exact synthesis procedure appear to be dim. Thus the synthesis procedure given here involves a number of simplifying approximations that permit straightforward, easy-to-use design calculations. Although the design formulas are approximate, the results of our trial designs indicate that they are sufficiently accurate for most practical applications.

For the benefit of readers who have filter design requirements but who are not particularly interested in filter theory as such, the design equations for interdigital filters and their practical use will be discussed first.
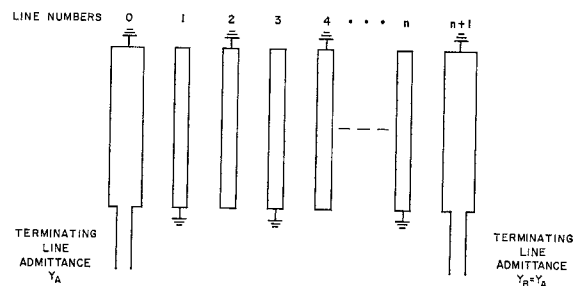

Fig. 1—Interdigital filter with short-circuited lines at the ends.
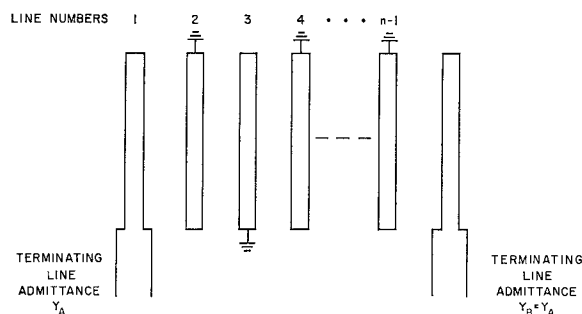

Fig. 2—Interdigital filter with open-circuited lines at the ends.

Readers who are also interested in knowing where the design equations came from will find a discussion of their derivation in Section VI.

II. Low-Pass Prototype Filters and Use of a Low-Pass-to-Band-Pass Transformation

The design procedures to be described are based on the use of low-pass prototype filter element values to give the band-pass filter its desired characteristics. Fig. 3 shows typical low-pass prototypes of the type under discussion, and it also defines the manner in which the element values g_k are to be specified for the purpose of this discussion. The left side of Fig. 4 shows a typical Chebyshev response such as can be achieved by filters of this type. Element values for prototype filters having such responses have been tabulated.[7],[8] Notice that n is the number of reactive elements and that, including the resistor terminations, the element values range from g_0 to g_{n+1}. A low-pass prototype with n reactive elements leads to a band-pass filter with n resonators.

The right side of Fig. 4 shows a band-pass filter response which corresponds to the given low-pass prototype response. The band-pass filter response will have the same type of pass-band characteristic as the prototype, but the width of the band-pass filter pass band can

[5] S. B. Cohn, "Parallel-coupled transmission-line-resonator filters," IRE TRANS. ON MICROWAVE THEORY AND TECHNIQUES, vol. MTT-6, pp. 223–231; April, 1958.

[6] G. L. Matthaei, "Design of wide-band (and narrow-band) bandpass microwave filters on the insertion loss basis," IRE TRANS. ON MICROWAVE THEORY AND TECHNIQUES, vol. MTT-8, pp. 580–593; November, 1960.

[7] L. Weinberg, "Additional tables for design of optimum ladder networks," J. Franklin Inst., vol. 246, pp. 7–23, 127–138; July and August, 1957.

[8] G. L. Matthaei, et al., "Design Criteria for Microwave Filters and Coupling Structures," Stanford Res. Inst., Menlo Park, Calif., Final Rept., SRI Project 2326, Contract DA 36-039 SC-74862; January, 1961.
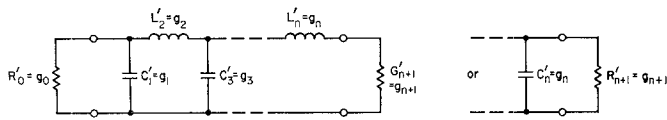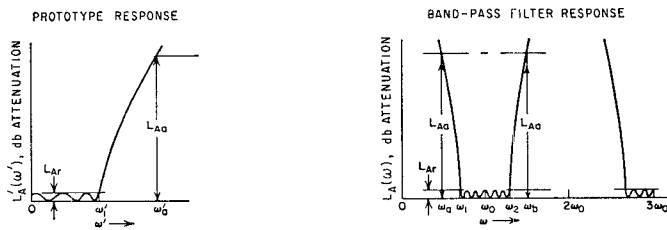
Fig. 3—Definition of prototype filter parameters g_0, g_1, g_2, $\cdots$, g_n, g_{n+1}. An additional prototype parameter ω_1' is defined in Fig. 4.

$$L_A(\omega) = L_A'(\omega') \text{ db} \qquad \omega_0 = \frac{\omega_2 + \omega_1}{2}$$

where

$$\omega' = \frac{2\omega_1'}{w} \left| \frac{\omega - \omega_0}{\omega_0} \right| \quad \text{and} \quad w = \frac{\omega_2 - \omega_1}{\omega_0}.$$

Fig. 4—Relation between the low-pass prototype response and the band-pass filter response.

be specified arbitrarily. Note that the band-pass filter response has arithmetic symmetry, and that it will repeat with pass bands centered at ω_0, $3\omega_0$, $5\omega_0$, etc. In Matthaei[6] will be found equations for determining the attenuation characteristics of maximally flat and Chebyshev low-pass prototype filters as a function of the radian frequency variable ω', for specified ω_1' and n. At the bottom of Fig. 4 will be found a low-pass-to-band-pass transformation from which the attenuation characteristic of the low-pass prototype as a function of ω' can be mapped to the band-pass filter attenuation characteristic (centered at ω_0) as a function of the band-pass filter radian frequency variable ω. Since the attenuation is the same for both the low-pass and band-pass filters at frequencies ω' and ω, respectively, which are related as given by the mapping, the band-pass filter attenuation characteristic can be predicted by use of these data. Matthaei[6] contains equations for determining the value of n required in order to achieve a given amount of attenuation, L_{Aa} db, at a given frequency, ω_a.

The low-pass-to-band-pass transformation given in Fig. 4 is an approximate one and is usually considered to be useful only for filters of narrow or moderate bandwidth. However, it appears to work well for interdigital filters even in cases of quite large bandwidth, as is verified by the nearly octave bandwidth design discussed in Section V. The parameter w, which appears in the mapping equation, is the fractional bandwidth of the filter. This parameter will also be used in the filter design equations that are about to be presented. Our experience indicates that, because the design equations are based on various approximations, the actual fractional bandwidth of the filter will be about 7 per cent smaller than the value of w used in the equations. Thus to allow

for this shrinkage in bandwidth, it is suggested that a value of w, which is about 7 per cent larger than is actually desired, be used in the design equations in Sections IV and V. However, the actual desired value of w should be used in the mapping in Fig. 4.

III. PARALLEL-COUPLED LINES

As previously mentioned, interdigital filters consist of arrays of parallel lines between ground planes. The design equations for such filters to be given herein will yield the various line capacitances per unit length for the various lines in the filter array. From these values of capacitance per unit length, the actual dimensions of the lines can be determined. Definitions for these various line capacitances will now be given, and also equations for obtaining the line dimensions from the specified capacitances. In order to relate the design methods under discussion to existing design data that are extremely useful when adapted for the design of arrays of parallel lines, we will first consider the case of two unsymmetrical parallel-coupled lines. (The case of two parallel-coupled lines will also be of interest in Section VI, where the derivation of the design equations for interdigital filters will be explained.)

Case of Two Unsymmetrical Parallel-Coupled Lines

Fig. 5 shows an unsymmetrical pair of parallel-coupled lines and various line capacitances. Note that C_a is the capacitance per unit length between Line a and ground, C_{ab} is the capacitance per unit length between Line a and Line b; and C_b is the capacitance per unit length between Line b and ground. When C_a is not equal to C_b, the two lines will have different odd- and even-mode admittances as is indicated by (a) in Table I. In terms of odd- and even-mode capacitances, for Line a[9-11]

$$C_{oo}{}^a = C_a + 2C_{ab}, \qquad C_{oe}{}^a = C_a \tag{1}$$

while for Line b

$$C_{oo}{}^b = C_b + 2C_{ab}, \qquad C_{oe}{}^b = C_b. \tag{2}$$

For symmetrical parallel-coupled lines the odd-mode impedances are simply the reciprocals of the odd-mode admittances, and analogously for the even-mode impedances and admittances. However, as can be demonstrated from (b) in Table I, this is not the case for unsymmetrical parallel-coupled lines. For unsymmetrical lines, the odd- and even-mode impedances are not simply the reciprocals of the odd- and even-mode ad-

[9] S. B. Cohn, "Shielded coupled-strip transmission line," IRE TRANS. ON MICROWAVE THEORY AND TECHNIQUES, vol. MTT-3, pp. 29–38; October, 1955.

[10] W. J. Getsinger, "Coupled rectangular bars between parallel plates," IRE TRANS. ON MICROWAVE THEORY AND TECHNIQUES, vol. MTT-10, pp. 65–72; January, 1962.

[11] E. M. T. Jones and J. T. Bolljahn, "Coupled-strip-transmission-line filters and directional couplers," IRE TRANS. ON MICROWAVE THEORY AND TECHNIQUES, vol. MTT-4, pp. 75–81; April, 1956.
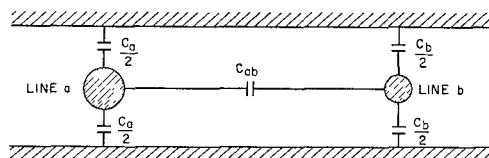
Fig. 5—An unsymmetrical pair of parallel-coupled lines (C_a, C_{ab}, and C_b are line capacitances per input length).

Fig. 6—Cross section of unsymmetrical, rectangular-bar parallel-coupled lines.

TABLE I

RELATIONS BETWEEN LINE ADMITTANCES, IMPEDANCES, AND
CAPACITANCES PER UNIT LENGTH OF UNSYMMETRICAL
PARALLEL-COUPLED LINES

v = velocity of light in medium of propagation

$\quad = 1.18 \times 10^{10}/\sqrt{\epsilon_r}$ inches/sec.

η_0 = intrinsic impedance of free space = 376.7 ohms

ϵ = dielectric constant = $0.225\epsilon_r\ \mu\mu f$/inch

$$
\left.
\begin{aligned}
Y_{oe}{}^a &= vC_a, & Y_{oo}{}^a &= v(C_a + 2C_{ab}) \\
Y_{oe}{}^b &= vC_b, & Y_{oo}{}^b &= v(C_b + 2C_{ab})
\end{aligned}
\right\} \quad \text{(a)}
$$

$$
\left.
\begin{aligned}
Z_{oe}{}^a &= \frac{C_b + 2C_{ab}}{vF}, & Z_{oo}{}^a &= \frac{C_b}{vF} \\
Z_{oe}{}^b &= \frac{C_a + 2C_{ab}}{vF}, & Z_{oo}{}^b &= \frac{C_a}{vF}
\end{aligned}
\right\} \quad \text{(b)}
$$

where $F = C_a C_b + C_a C_{ab} + C_b C_{ab}$

$$
\left.
\begin{aligned}
\frac{C_a}{\epsilon} &= \frac{\eta_0 Y_{oe}{}^a}{\sqrt{\epsilon_r}}, & \frac{C_{ab}}{\epsilon} &= \frac{\eta_0}{\sqrt{\epsilon_r}}\left(\frac{Y_{oo}{}^a - Y_{oe}{}^a}{2}\right) \\
\frac{C_b}{\epsilon} &= \frac{\eta_0 Y_{oe}{}^b}{\sqrt{\epsilon_r}}, & \frac{C_{ab}}{\epsilon} &= \frac{\eta_0}{\sqrt{\epsilon_r}}\left(\frac{Y_{oo}{}^b - Y_{oe}{}^b}{2}\right)
\end{aligned}
\right\} \quad \text{(c)}
$$

$$
\left.
\begin{aligned}
\frac{C_a}{\epsilon} &= \frac{\eta_0 2 Z_{oo}{}^b}{\sqrt{\epsilon_r}H}, & \frac{C_{ab}}{\epsilon} &= \frac{\eta_0}{\sqrt{\epsilon_r}}\left(\frac{Z_{oe}{}^b - Z_{oo}{}^b}{H}\right) \\
\frac{C_b}{\epsilon} &= \frac{\eta_0 2 Z_{oo}{}^a}{\sqrt{\epsilon_r}H}, & \frac{C_{ab}}{\epsilon} &= \frac{\eta_0}{\sqrt{\epsilon_r}}\left(\frac{Z_{oe}{}^a - Z_{oo}{}^a}{H}\right)
\end{aligned}
\right\} \quad \text{(d)}
$$

where $H = Z_{oe}{}^a Z_{oo}{}^b + Z_{oe}{}^b Z_{oo}{}^a$.

mittances. The reason for this lies in the fact that when the odd- and even-mode *admittances* are computed, the basic definition of these admittances assumes that the lines are being driven with *voltages of identical magnitude* with equal or opposite phase, while the *currents* in the lines may be of different magnitudes.[11] When the odd- and even-mode *impedances* are computed, the basic definition of these impedances assumes that the lines are being driven by *currents of identical magnitude* with equal or opposite phases,[11] while magnitudes of the *voltages* on the two lines may be different. These two different sets of boundary conditions can be seen to lead to different voltage-current ratios if the lines are unsymmetrical.

Some unsymmetrical parallel-coupled lines that are quite easy to design are shown in Fig. 6. Note that the capacitance per unit length of each line has been separated into component parts. The capacitance $C_p{}^a$ is the *parallel plate* capacitance per unit length between one side of Line a and the adjacent ground plane, while $C_p{}^b$ is the corresponding *parallel plate* capacitance of Line b. The capacitance $C_f{}'$ is the fringing capacitance per unit length for any of the outer corners of the striplines. The
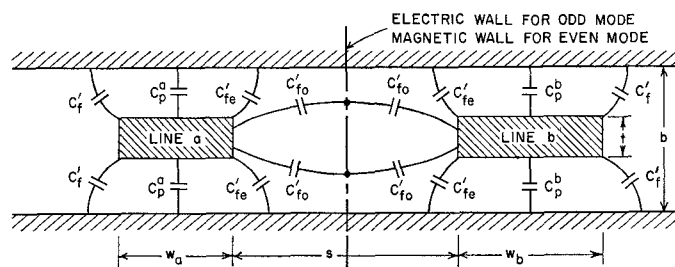
fringing capacitances per unit length at the inner corners of each strip are designated $C_{fe}{}'$ when the strips are excited in the even mode (*i.e.*, with equal voltages of the same phase); they are designated $C_{fo}{}'$ when the strips are excited in the odd mode (*i.e*, with voltages having equal amplitudes and opposite phases). Both bars have the same height, and both are assumed to be wide enough that the interactions between the fringing fields at the right and left sides of each bar are negligible, or at least small enough to be easily corrected for. On this basis the fringing fields are the same for both bars, and their different capacitances C_a and C_b to ground are due entirely to different parallel plate capacitances $C_p{}^a$ and $C_p{}^b$. For the structure shown

$$
\begin{aligned}
C_a &= 2(C_p{}^a + C_f{}' + C_{fe}{}') \\
C_{ab} &= (C_{fo}{}' - C_{fe}{}') \\
C_b &= 2(C_p{}^b + C_f{}' + C_{fe}{}').
\end{aligned}
\quad \text{(3)}
$$

Getsinger[10] has derived equations for the fringing capacitances $C_{fe}{}'$, $C_{fo}{}'$, and $C_f{}'$, and has prepared convenient charts which relate $C_{fe}{}'/\epsilon$, $C_{fo}{}'/\epsilon$, and $C_f{}'/\epsilon$ to rectangular-bar strip-line dimensions. Here ϵ is the dielectric constant of the medium of propagation, so that the above ratios are dimensionless and of moderate size. Getsinger gives equations for the design of *symmetrical*, parallel-coupled, rectangular strip-lines, and here we will adapt his equations to fit the unsymmetrical case.

Note that the shape of the lines in Fig. 6 is fixed in terms of the dimensions t, b, s, w_a and w_b. To design a pair of lines such as those in Fig. 6 so as to have specified odd- and even-mode admittances or impedances, first use (c) or (d) in Table I to compute C_a/ϵ, C_{ab}/ϵ, and C_b/ϵ. Select a convenient value for t/b, and noting that

$$
\frac{\Delta C}{\epsilon} = \frac{C_{ab}}{\epsilon}, \quad \text{(4)}
$$

use Getsinger's chart[10] of $\Delta C/\epsilon$ and $C_{fe}{}'/\epsilon$ vs s/b to determine s/b, and also $C_{fe}{}'/\epsilon$. Using t/b and Getsinger's chart of $C_f{}'/\epsilon$ vs t/b, determine $C_f{}'/\epsilon$, and then compute

$$
\frac{w_a}{b} = \frac{1}{2}\left(1 - \frac{t}{b}\right)\left[\frac{1}{2}\left(\frac{C_a}{\epsilon}\right) - \frac{C_{fe}{}'}{\epsilon} - \frac{C_f{}'}{\epsilon}\right] \quad \text{(5)}
$$

$$
\frac{w_b}{b} = \frac{1}{2}\left(1 - \frac{t}{b}\right)\left[\frac{1}{2}\left(\frac{C_b}{\epsilon}\right) - \frac{C_{fe}{}'}{\epsilon} - \frac{C_f{}'}{\epsilon}\right]. \quad \text{(6)}
$$

When the ground plane spacing b is specified, the required bar widths, w_a and w_b, are determined. This procedure also works for the thin-strip case where $t/b = 0$. If either w_a/b or w_b/b is less than $0.35\,(1 - t/b)$, the width of the bar should be corrected using the approximate formula[10]

$$\frac{w'}{b} = \frac{0.07\left(1 - \dfrac{t}{b}\right) + \dfrac{w}{b}}{1.20}, \qquad (7)$$

provided that $0.1 < (w'/b)/(1 - t/b) < 0.35$. In (7) w is the uncorrected bar width and w' is the corrected width. The need for this correction arises because of the interaction of the fringing fields at opposite sides of a bar, which will occur when a bar is relatively narrow.

Case of an Array of Parallel-Coupled Lines

Fig. 7 shows an array of parallel-coupled lines such as is used in an interdigital filter. In the structure shown, all of the bars have the same t/b ratio and the other dimensions of the bars are easily obtained by generalizing the procedure just described for designing unsymmetrical parallel-coupled lines. In the structure in Fig. 7 the electrical properties of the structure are characterized in terms of the self-capacitances, C_k, per unit length of each bar with respect to ground, and the mutual capacitances, $C_{k,k+1}$, per unit length between adjacent bars k and $k+1$. This representation is not necessarily always highly accurate; it is conceivable that a significant amount of fringing capacitance could exist between a given line element and, say, the line element beyond the nearest neighbor. However, at least for geometries such as that shown, experience has shown this representation to have satisfactory accuracy.

For the design of the interdigital filter structures discussed herein, equations will be given for the normalized self-and mutual capacitances, C_k/ϵ and $C_{k,k+1}/\epsilon$, per unit length for all the lines in the structure. Then the cross-sectional dimensions of the bars and spacings between them are determined as follows. First choose values for t and b. Then, since

$$\frac{(\Delta C)_{k,k+1}}{\epsilon} = \frac{C_{k,k+1}}{\epsilon}, \qquad (8)$$

Getsinger's charts can be used to determine $s_{k,k+1}/b$. In this manner, the spacings $s_{k,k+1}$ between all the bars are obtained. Also, using Getsinger's charts, the normalized fringing capacitance $(C_{fe}')_{k,k+1}/\epsilon$ associated with the gaps $s_{k,k+1}$ between bars are obtained. Then the normalized width of the kth bar is

$$\frac{w_k}{b} = \frac{1}{2}\left(1 - \frac{t}{b}\right)$$
$$\cdot\left[\frac{1}{2}\left(\frac{C_k}{\epsilon}\right) - \frac{(C_{fe}')_{k-1,k}}{\epsilon} - \frac{(C_{fe}')_{k,k+1}}{\epsilon}\right]. \qquad (9)$$
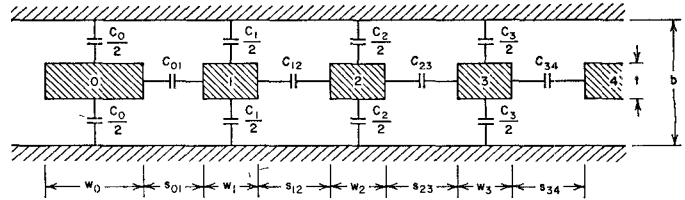

Fig. 7—Cross section of an array of parallel-coupled lines between ground planes.

In the case of the bar at the end of the array (the bar at the far left in Fig. 7), C_{fe}'/ϵ for the edge of the bar that has no neighbor must be replaced by C'_f, which is also obtained from Getsinger's charts. Thus, for example, for Bar 0 in Fig. 7

$$\frac{w_0}{b} = \frac{1}{2}\left(1 - \frac{t}{b}\right)\left[\frac{1}{2}\left(\frac{C_0}{\epsilon}\right) - \frac{C_f'}{\epsilon} - \frac{(C_{fe}')_{01}}{\epsilon}\right]. \qquad (10)$$

If $w_k/b < 0.35\,(1 - t/b)$ for any of the bars, the width correction given in (7) should be applied to the affected bars.

IV. Interdigital Filters of Narrow or Moderate Bandwidth

Table II shows approximate design equations for interdigital filters of the form shown in Fig. 1. This type of design is most practical for filters having narrow or moderate bandwidth. Although no special investigation of this point has been made, it appears probable that one should consider the possibility of using the design equations in Section V when the bandwidth is of the order of 30 per cent or more, instead of those in Table II. Both sets of design equations are valid, however, for either narrow or wide bandwidths. The main drawback in applying the design procedure in this section to filters of wide bandwidth is that the gaps between Lines 0 and 1 and between Lines n and $n+1$ (see Fig. 1) tend to become inconveniently small when the bandwidth is large, and the widths of Bars 1 and n tend to become very small.

To use Table II for the design of an interdigital filter, first use the mapping in Fig. 4 to estimate the number n of reactive elements required in the low-pass prototype in order to give the desired rate of cutoff with the desired pass-band characteristics.[6] When the prototype cutoff frequency ω_1' and element values $g_0, g_1, \cdots, g_{n+1}$ have been obtained from tables[7,8] or by computations,[12] the design computations can begin. It is suggested that the filter fractional bandwidth w be specified to be 6 or 7 per cent larger than is actually desired since, from our experience, there will be some shrinkage in bandwidth due to the approximate nature of the design equations. However, the desired value of w should be used in the mapping in Fig. 4.

After all of the J/Y_A and N parameters in Table II

[12] S. B. Cohn, "Direct-coupled-resonator filters," Proc. IRE, vol. 45, pp. 187–196; February, 1957.

TABLE II

DESIGN EQUATIONS FOR INTERDIGITAL FILTERS
OF THE FORM IN FIG. 1

Use mapping in Fig. 4 to select a low-pass prototype with the required value of n. The input and output lines in this filter do not count as resonators, so that there are $n+2$ lines for an n-reactive-element prototype.

Compute

$$\theta_1 = \frac{\pi}{2}\frac{\omega_1}{\omega_0} = \frac{\pi}{2}\left(1 - \frac{u}{2}\right)$$

$$\frac{J_{01}}{Y_A} = \frac{1}{\sqrt{g_0 g_1 \omega_1'}}, \qquad \frac{J_{k,k+1}}{Y_A}\bigg|_{k=1 \text{ to } n-1} = \frac{1}{\omega_1'\sqrt{g_k g_{k+1}}}$$

$$\frac{J_{n,n+1}}{Y_A} = \frac{1}{\sqrt{g_n g_{n+1}\omega_1'}},$$

$$N_{k,k+1}\bigg|_{k=1 \text{ to } n-1} = \sqrt{\left(\frac{J_{k,k+1}}{Y_A}\right)^2 + \frac{\tan^2\theta_1}{4}},$$

$$M_1 = Y_A\left[\frac{J_{01}}{Y_A}\sqrt{h} + 1\right], \qquad M_n = Y_A\left[\frac{J_{n,n+1}}{Y_A}\sqrt{h} + 1\right]$$

where h is a dimensionless admittance scale factor to be specified arbitrarily so as to give a convenient admittance level in the filter. (See text.)

The normalized self-capacitances C_k/ϵ per unit length for the line elements are

$$\frac{C_0}{\epsilon} = \frac{376.7}{\sqrt{\epsilon_r}}\left[2Y_A - M_1\right]$$

$$\frac{C_1}{\epsilon} = \frac{376.7}{\sqrt{\epsilon_r}}\left[Y_A - M_1 + hY_A\left[\frac{\tan\theta_1}{2} + \left(\frac{J_{01}}{Y_A}\right)^2 + N_{12} - \frac{J_{12}}{Y_A}\right]\right]$$

$$\frac{C_k}{\epsilon}\bigg|_{k=2 \text{ to } n-1} = \frac{376.7}{\sqrt{\epsilon_r}}hY_A\left[N_{k-1,k} + N_{k,k+1} - \frac{J_{k-1,k}}{Y_A} - \frac{J_{k,k+1}}{Y_A}\right]$$

$$\frac{C_n}{\epsilon} = \frac{376.7}{\sqrt{\epsilon_r}}\left[Y_A - M_n + hY_A\left[\frac{\tan\theta_1}{2} + \left(\frac{J_{n,n+1}}{Y_A}\right)^2 + N_{n-1,n} - \frac{J_{n-1,n}}{Y_A}\right]\right]$$

$$\frac{C_{n+1}}{\epsilon} = \frac{376.7}{\sqrt{\epsilon_r}}\left[2Y_A - M_n\right]$$

where ϵ is the dielectric constant and ϵ_r is the relative dielectric constant in the medium of propagation.

The normalized mutual capacitances $C_{k,k+1}/\epsilon$ per unit length between adjacent line elements are

$$\frac{C_{01}}{\epsilon} = \frac{376.7}{\sqrt{\epsilon_r}}\left[M_1 - Y_A\right],$$

$$\frac{C_{k,k+1}}{\epsilon}\bigg|_{k=1 \text{ to } n-1} = \frac{376.7 hY_A}{\sqrt{\epsilon_r}}\left(\frac{J_{k,k+1}}{Y_A}\right),$$

$$\frac{C_{n,n+1}}{\epsilon} = \frac{376.7}{\sqrt{\epsilon_r}}\left[M_n - Y_A\right].$$

have been computed, the admittance scale factor h must be fixed. One of the prime considerations in the choice of h is that the line dimensions must be such that the resonators will have a high unloaded Q. The dimensions that give optimum resonator Q's in structures such as interdigital filters are not known. However, it is known that for air-filled, coaxial-line resonators the optimum Q will result when the line impedance is about 76 ohms, and various approximate studies suggest that the optimum impedance for strip-line resonators is not greatly different. Thus it is suggested that in this case h be chosen to make the quantity

$$\frac{2C_{k-1,k}}{\epsilon} + \frac{C_k}{\epsilon} + \frac{2C_{k,k+1}}{\epsilon}\bigg|_{\substack{k=n/2 \text{ for } n \text{ even} \\ =(n+1)/2 \text{ for } n \text{ odd}}}$$

$$= (\text{around } 5.4) \tag{11}$$

if air dielectric is used. If the quantity in (11) is set equal to 5.4 for the case of $\epsilon_r = 1$, this corresponds to making the line impedance 70 ohms for the resonator lines in the center of the filter, under the conditions that the adjacent lines are being excited with the same amplitude of voltage but with opposite phase (this is a generalized odd-mode admittance condition). Having established a value for h, the remainder of the calculations follow in a straightforward manner. After the normalized capacitances C_k/ϵ and $C_{k,k+1}/\epsilon$ have been computed, the line dimensions are determined as discussed in Section III.

A trial design was worked out using an $n=6$ reactive-element Chebyshev prototype with $L_{Ar}=0.10$ db. The prototype parameters were $g_0=1$, $g_1=1.1681$, $g_2=1.4039$ $g_3=2.0562$, $g_4=1.5170$, $g_5=1.9029$, $g_6=0.8618$, $g_7=1.3554$, and $\omega_1'=1$. The design was worked out for a fractional bandwidth of $w=0.10$ centered at $f_0=1.5$ Gc. Table III summarizes the various parameters used or computed in the calculations. The parameter h was chosen so that (11) would be 5.4. The resulting circuit has symmetry in its dimensions because the Chebyshev prototype is antimetric (*i.e.*, one half of the network is reciprocal to the other half).[7]

TABLE III

TABULATION OF QUANTITIES IN TABLE II AND IN FIG. 7, FOR A 10 PER CENT BANDWIDTH TRIAL DESIGN

k	$J_{k,k+1}/Y_A$	$N_{k,k+1}$	$C_{k,k+1}/\epsilon$	$s_{k,k+1}$ (Inches)	k	C_k/ϵ	w_k (Inches)
0 and 6	0.9253		1.582	0.159*	0 and 7	5 950	0.405†
1 and 5	0.7809	6.401	0.301	0.419	1 and 6	3.390	0.152
2 and 4	0.5886	6.381	0.226	0.512	2 and 5	4.420	0.183
3	0.5662	6.379	0.218	0.520	3 and 4	4.496	0.183

$w=0.10$ $Y_A = 0\ 020$ mho
$\theta_1=1.492$ $M_1 = M_6 = 0.02420$
$h=0.05143$ $b=0.625$ inch
$\epsilon_r=1$ $t=0.187$ inch

* Changed to 0.127 inch after laboratory tests.
† Changed to 0.437 inch after laboratory tests.

Fig. 8 shows a photograph of the completed filter, while Fig. 9 shows those dimensions of the filter not summarized in Table III. The short-circuiting side walls of the structure are spaced exactly a quarter-wavelength apart at the midband frequency $f_0 = 1.5$ Gc ($\lambda_0/4 = 1.968$ in). Because of the capacitance between the open-circuited ends of the resonator elements and the side walls, it was necessary to foreshorten the resonators so as to maintain their resonant frequency at 1.5Gc. No very satisfactory means for accounting for all of the fringing capacitances at the open-circuit ends of the reasonators has been devised, but some rough estimates were made using Getsinger's fringing data[10] and various

Fig. 8—A 10 per cent bandwidth interdigital filter with its cover plate removed.

Fig. 9—Drawing of the 10 per cent bandwidth interdigital filter (part of the dimensions are as specified by Table III and Fig. 7).

approximations. The estimated foreshortening for the resonators was 0.216 inch, but laboratory tests showed this to be excessive since the pass-band center was 1.56 instead of 1.50 Gc. Although the filter pass band can always be lowered in frequency by use of tuning screws, if the resonators had been foreshortened by about 0.160 inch instead of 0.216 inch, the pass-band center frequency would probably have been about right.

Although the structure included tuning screws, no effort was made to lower the band center frequency to 1.50 Gc. However, it was found that since Resonators 1 and 6 have different fringing capacitance conditions at their open-circuit ends than do the other resonators, it was necessary to increase the capacitance at their open-circuit ends by inserting the tuning screws. Before this was done, the pass-band response was not symmetrical (this is indicative of mistuning of some of the resonators with respect to the others).

When the filter was first tested the pass-band VSWR reached peaks of 2.2, which is somewhat high since 0.1-db Chebyshev ripples call for VSWR peaks of only 1.36. Such conditions can usually be corrected by altering the couplings between the terminations and the first resonator on each end. Thus, a 0.032-inch-thick brass shim was added to the input and output lines (Lines 0 and 7) to reduce the adjacent gaps from $s_{01} = s_{67} = 0.159$ inch to 0.127 inch. This reduced the input VSWR to 1.30 or less across the band. It appears desirable that in working out the design of trial models of interdigital filters as described herein, some provision should be made for experimental adjustment of the size of coupling gaps at the ends, if the pass-band VSWR is to be closely controlled.

Fig. 10 shows the measured attenuation characteristic of this filter, while Fig. 11 shows the measured VSWR. The measured fractional band width is slightly less than the design value ($w = 0.0935$ instead of 0.100). Using $w = 0.0935$ and $f_0 = \omega_0/(2\pi) = 1.563$ Gc the measured attenuation was compared with that computed by mapping the low-pass prototype attenuation as indicated in Fig. 4. The measured attenuation in the stop bands was found to be somewhat less than that predicted for a Chebyshev filter with $L_{Ar} = 0.1$-db ripple. However, the pass-band VSWR in Fig. 11 is, for the most part, much less than the 1.36 peak value corresponding to a 0.1-db Chebyshev ripple, and some of the VSWR amplitude shown may be due to the connectors and slight mistuning.[13] The attenuation for a $L_{Ar} = 0.01$-db ripple filter (VSWR = 1.1 peak) was also computed, and the results are summarized in Table IV. Note that in all cases the measured stop-band attenua-
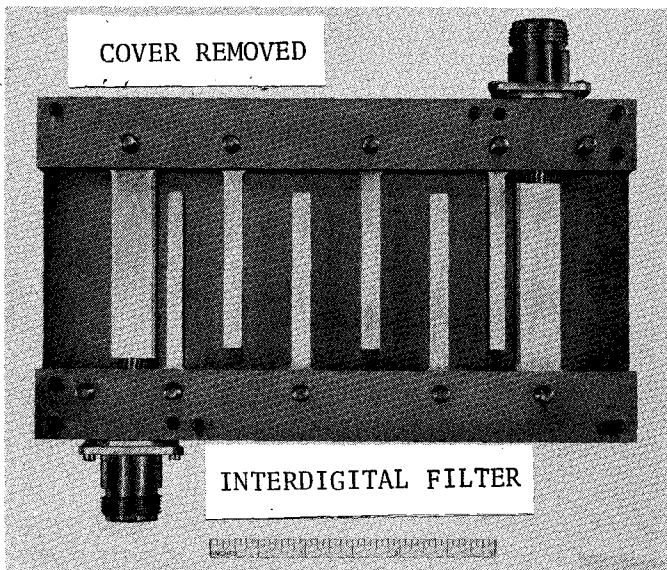
---
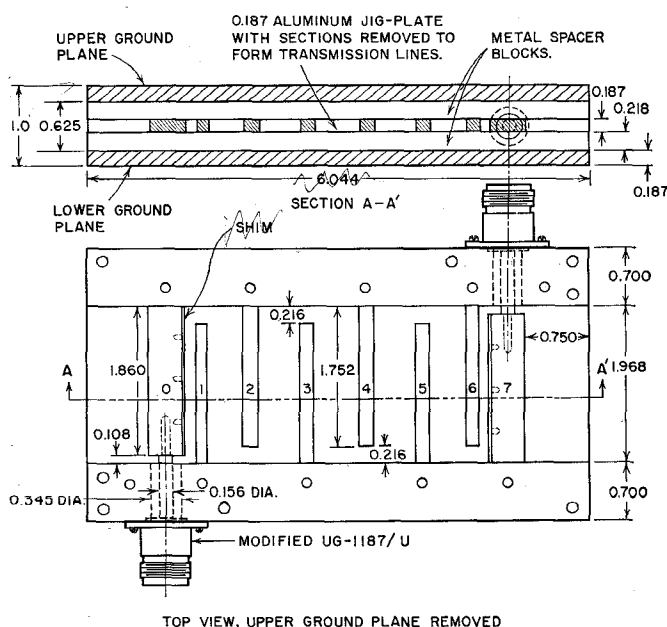
[13] The pass-band VSWR is the most sensitive index of the correlation of the actual design as compared to the pass-band characteristic of the prototype. The pass-band attenuation as determined from through transmission measurements includes the additional attenuation due to dissipation loss, which may be markedly greater than 0.1 db depending on the Q's of the resonators.
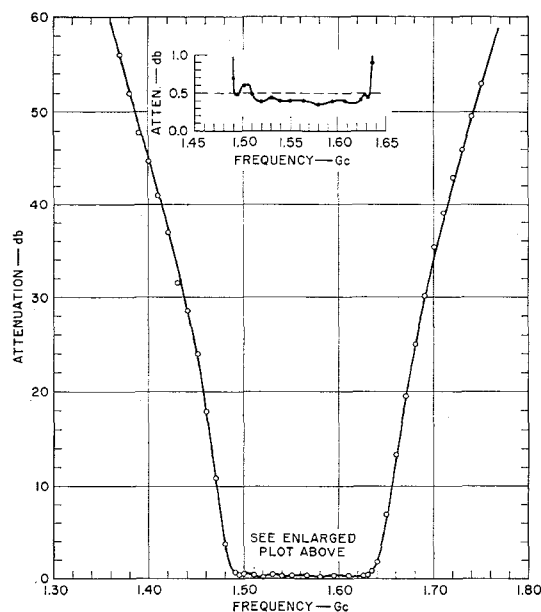
Fig. 10—Measured attenuation characteristic
of the filter in Fig. 8.
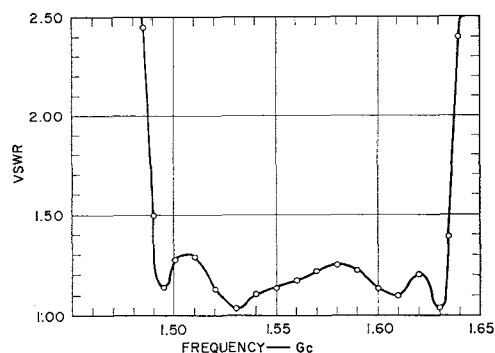
Fig. 11—Measured VSWR of the filter in Fig. 8.

TABLE IV

COMPARISON OF MEASURED ATTENUATION IN FIG. 10
WITH ATTENUATION PREDICTED AS IN FIG. 4

[Computed values are for 0.01- and 0.10-db ripple, $n = 6$,
$w = 0.0935$, and $f_0 = \omega_0/(2\pi) = 1.563$ Gc]

f, Gc	L_A, db for $L_A = 0.01$	L_A, db measured	L_A, db for $L_{Ar} = 0.10$
1.440	25	29	35.5
1.686	25	28	35.5
1.380	49.5	52	59.5
1.746	49.5	52	59.5

tion is less than that computed for a 0.10-db ripple filter, but more than that for a 0.01-db ripple filter. Thus the approximate mapping in Fig. 4 appears to be reasonably consistent with the measured results.

Calculating from the measured pass-band insertion loss, it is estimated that the unloaded Q's of the resonators in this filter are about 1100. Using copper for the structure instead of aluminum would theoretically give a value about 25 per cent higher for the unloaded Q's.

It is possible that a different impedance level within the filter might also give higher Q's for a given ground plane spacing.

The lines in the trial interdigital filter (Figs. 8 and 9) were fabricated by machining Lines 0, 2, 4, and 6 in comb form from a single piece of jig plate. Lines 1, 3, 5, and 7 were cut out similarly from a second piece of jig plate. (Actually, both comb structures were machined at once, back to back.) Then, interleaving the two comb structures between ground planes gave the desired interdigital structure.

Fig. 12 shows an alternative form of interdigital filter structure that should be even less expensive to fabricate. In this case the interdigital line structure is photoetched on a copper-clad dielectric card, and the dielectric material removed from the region between the copper-foil lines. In order to provide good support for the lines, the dielectric is not removed at the open-circuit ends of the lines, however. Using this structure the propagation is largely in air, which should permit good performance; also, the dielectric card line structures should be quite inexpensive to mass produce.

Round rods between ground planes also provide an attractive form for fabricating interdigital filters.[4] However, no data are yet available for accurate determination of the rod diameters and spacings from specified line capacitances.[14] Work on this problem is planned at SRI for the near future.
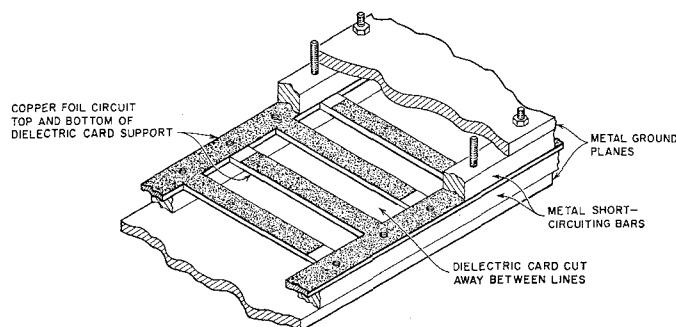
Fig. 12—A proposed low-cost construction
for interdigital lines filters.

V. INTERDIGITAL FILTERS OF MODERATE OR WIDE BANDWIDTH

Table V presents approximate design equations for filters of the form in Fig. 2. This type of filter is most practical for designs having moderate or wide bandwidths, although the design procedure given is valid for either narrow- or wide-band filters. The main drawback in applying the procedure in Table V to narrow-band filters is that Lines 1 and n will attain extremely high impedance in such designs.

[14] Bolljahn and Matthaei (4) give an approximate method for design of structures consisting of rods that are all the same size and have the same spacings. A procedure for accurate design where varying diameters and spacings are required has not as yet been obtained.

TABLE V

DESIGN EQUATIONS FOR INTERDIGITAL FILTERS OF
THE FORM IN FIG. 2

Use mapping in Fig. 4 to select low-pass prototype with the required value of n. The input and output lines in this filter count as resonators, so that there are n line elements for an n-reactive-element prototype. Compute

$$\theta_1 = \frac{\pi}{2}\frac{\omega_1}{\omega_0} = \frac{\pi}{2}\left(1 - \frac{w}{2}\right)$$

$$\left.\frac{J_{k,k+1}}{Y_A}\right|_{k=2 \text{ to } n-3} = \frac{g_2}{g_0\sqrt{g_k g_{k+1}}}, \qquad \frac{J_{n-2,n-1}}{Y_A} = \frac{1}{g_0}\sqrt{\frac{g_0 g_2}{g_{n-2}g_{n+1}}}$$

$$\left.N_{k,k+1}\right|_{k=2 \text{ to } n-2} = \sqrt{\left(\frac{J_{k,k+1}}{Y_A}\right)^2 + \left(\frac{\omega_1' g_2 \tan\theta_1}{2g_0}\right)^2}$$

$$\frac{Z_1}{Z_A} = \omega_1' g_0 g_1 \tan\theta_1$$

$$\frac{Y_2}{Y_A} = \frac{\omega_1' g_2}{2g_0}\tan\theta_1 + N_{23} - \frac{J_{23}}{Y_A}$$

$$\left.\frac{Y_k}{Y_A}\right|_{k=3 \text{ to } n-2} = N_{k-1,k} + N_{k,k+1} - \frac{J_{k-1,k}}{Y_A} - \frac{J_{k,k+1}}{Y_A}$$

$$\frac{Y_{n-1}}{Y_A} = \frac{\omega_1'(2g_0 g_{n-1} - g_2 g_{n+1})\tan\theta_1}{2g_0 g_{n+1}} + N_{n-2,n-1} - \frac{J_{n-2,n-1}}{Y_A}$$

$$\frac{Z_n}{Z_A} = \omega_1' g_n g_{n+1} \tan\theta_1.$$

The normalized self-capacitances, C_k/ϵ, per unit length for the line elements are

$$\frac{C_1}{\epsilon} = \frac{367.7}{\sqrt{\epsilon_r}} Y_A \frac{(1 - \sqrt{h})}{(Z_1/Z_A)}$$

$$\frac{C_2}{\epsilon} = \frac{376.7}{\sqrt{\epsilon_r}} Y_A h\left(\frac{Y_2}{Y_A}\right) - \sqrt{h}\frac{C_1}{\epsilon}$$

$$\left.\frac{C_k}{\epsilon}\right|_{k=3 \text{ to } n-2} = \frac{376.7}{\sqrt{\epsilon_r}} Y_A h\left(\frac{Y_k}{Y_A}\right)$$

$$\frac{C_{n-1}}{\epsilon} = \frac{376.7}{\sqrt{\epsilon_r}} Y_A h\left(\frac{Y_{n-1}}{Y_A}\right) - \sqrt{h}\frac{C_n}{\epsilon}$$

$$\frac{C_n}{\epsilon} = \frac{376.7}{\sqrt{\epsilon_r}} Y_A \frac{(1 - \sqrt{h})}{(Z_n/Z_A)}$$

where ϵ is the dielectric constant, ϵ_r is the relative dielectric constant in the medium of propagation, and h is a dimensionless admittance scale factor whose value should be chosen to give a convenient admittance level in the filter. (See Text.)

The normalized mutual capacitances $C_{k,k+1}/\epsilon$ per unit length between adjacent line elements are

$$\frac{C_{12}}{\epsilon} = \frac{376.7}{\sqrt{\epsilon_r}} Y_A \frac{\sqrt{h}}{(Z_1/Z_A)}$$

$$\left.\frac{C_{k,k+1}}{\epsilon}\right|_{k=2 \text{ to } n-2} = \frac{376.7}{\sqrt{\epsilon_r}} Y_A h\left(\frac{J_{k,k+1}}{Y_A}\right)$$

$$\frac{C_{n-1,n}}{\epsilon} = \frac{376.7}{\sqrt{\epsilon_r}} Y_A \frac{\sqrt{h}}{(Z_n/Z_A)}.$$

Except for the somewhat different design equations, the procedure for the design of filters of the form shown in Fig. 2 is much the same as that described for filters of the form shown in Fig. 1. It is suggested that for use in Table V, w be made about 8 per cent larger than the actual desired fractional bandwidth, in order to allow for some bandwidth shrinkage. Eq. (11) is applicable when selecting a value for the admittance scale factor h.

A trial design was worked out using an $n=8$ reactive-element Chebyshev prototype with $L_{Ar}=0.10$ db. The prototype parameters were $g_0=1$, $g_1=1.1897$, $g_2=1.4346$, $g_3=1.1199$, $g_4=1.6010$, $g_5=2.1699$, $g_6=1.5640$, $g_7=1.9444$ $g_8=0.8778$, $g_9=1.3554$, and $\omega_1'=1$. The design was carried out for a fractional bandwidth of $w=0.70$ centered at 1.50 Gc, and the parameter h was chosen to make (11) equal to 5.86. (This gives a generalized odd-mode impedance of 64.5 ohms for the middle lines.) Table VI summarizes some of the quantities computed in the course of the design of this filter.

Fig. 13 shows the completed filter, while the drawing in Fig. 14 shows additional construction details and additional dimensions not summarized in Table VI. The filter was fabricated in much the same manner as the filter described in Section IV, except that the resonator lines were foreshortened by 0.150 inch. The relatively small cross-sectional dimensions of the resonator elements, unfortunately, made 0.150 inch excessive, so that the measured band center frequency was 1.55 Gc instead of 1.50 Gc. It is probable that foreshortening the line elements about 0.125 inch would have been about right.

When this filter was first tested, the VSWR was quite low across the band (about 1.2 or less) except at band center where the VSWR peaked to 1.8. This situation was altered by increasing the s_{12} and s_{78} gaps from 0.087 inch to 0.092 inch, which caused the VSWR peaks across the band to be more nearly even and to be 1.55 or less.

Fig. 15 shows the measured attenuation of this filter, while Fig. 16 shows its measured VSWR. The fractional bandwidth is 0.645 instead of the specified 0.700 value, which indicates a shrinkage of bandwidth of about 8 per cent, as a result of the various approximations involved in the design equations. The attenuation characteristics in Fig. 15 were checked against the attenuation computed using the mapping in Fig. 4 with $w=0.645$, $L_{Ar}=0.10$ db, $n=8$, and $f_0=\omega_0/(2\pi)=1.55$ Gc. The resulting computed values are listed in Table VII along with the corresponding measured values of attenuation. The agreement can be seen to be quite good.

VI. CONCERNING THE DERIVATION OF THE DESIGN EQUATIONS

The design equations presented for interdigital filters were obtained by extending a previously discussed theory[6] for band-pass microwave filter design. Since much of the relevant theory has been explained before, only the necessary extensions of the previous theory will be treated.

Design theory has been presented for filters of the form in Fig. 17 which consist of parallel-coupled resonators which are $\lambda_0/2$ long at the midband frequency.[6] There is a $\lambda_0/4$, short-circuit input and output coupling line at each end of this filter; these are designed to serve as part of an admittance-transforming section. An in-

TABLE VI

TABULATION OF SOME OF THE PARAMETERS COMPUTED IN THE DESIGN OF THE TRIAL OCTAVE-BANDWIDTH INTERDIGITAL FILTER

(The dimensions are as defined in Fig. 7)

k	$J_{k,k+1}/Y_A$	$C_{k,k+1}/\epsilon$	$S_{k,k+1}$ (inches)	k	$\dfrac{Z_k}{Z_A}$ or $\dfrac{Y_k}{Y_A}$	C_k/ϵ	w_k (inches)
1 and 7		1.647	0.087*	1 and 8	1.941	2.235	0.126†
2 and 6	0.823	1.115	0.136	2 and 7	1.779	1.463	0.121†
3 and 5	0.779	1.056	0.143	3 and 6	1.235	1.675	0.126†
4	0.770	1.044	0.146	4 and 5	1.258	1.706	0.127†

$w = 0.70$ $Y_A = 0.020$ mho
$\theta_1 = 1.021$ $b = 0.625$ inch
$h = 0.18$ $t = 0.063$ inch
$\epsilon_r = 1$

* Changed to 0.092 inch after laboratory tests.
† Computed using Eq. (7) for width correction.
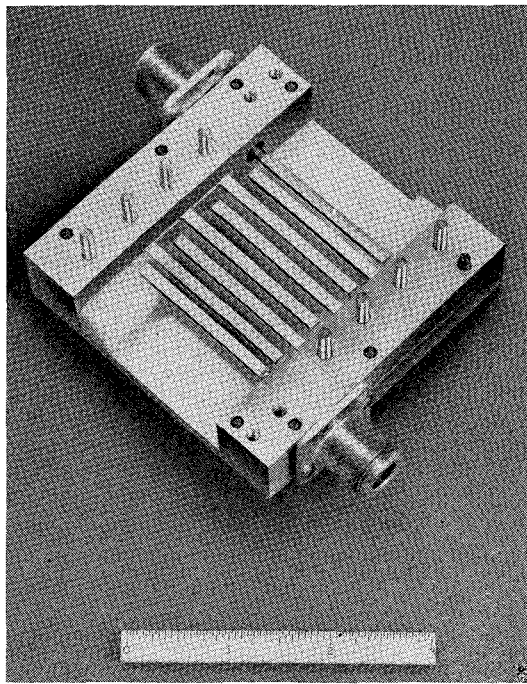
Fig. 13—Octave bandwidth interdigital filter
with cover plate removed.

Fig. 14—Drawing of the interdigital filter in Fig. 13 (other dimensions not shown are as defined by Fig. 7 and Table VI).

terdigital filter of the form in Fig. 1 is obtained from the filter in Fig. 17 if each $\lambda_0/2$ line is cut in the middle and folded double to give the structure in Fig. 18. It can be seen from Fig. 19 that this operation has little effect on the currents and voltages on the lines—at least at mid-band. Fig. 19(a) shows the voltages and currents on a short-circuited $\lambda_0/2$ resonator, while Fig. 19(b) shows the voltages and currents after the resonator has been cut and folded. Note that the voltages and currents on the a and b portions of the resonator are the same in either case.

The circuits in Figs. 17 and 18 are clearly not electrically the same. First, if the structure in Fig. 18 has significant fringing capacitances extending beyond nearest-neighbor line elements, the coupling mechanism would become much more complicated than is implied by the simple folding process. Second, the circuit in Fig. 17 can be shown to have only a first-order pole of attenuation at $\omega = 0$, $2\omega_0$, $4\omega_0$, etc.,[6] while the circuit in Fig. 18 has high-order poles of attenuation at these frequencies. For this reason it was believed that folding a filter as in Fig. 18 would have very little effect on its response for frequencies near ω_0 (provided that fringing beyond nearest neighbors is negligible), but that the error might be considerable at frequencies well removed from ω_0 (which would imply that the folding shown in Fig. 18 might considerably disturb the response of a wide-band filter). To check this point, the image cutoff frequency predicted by the approximation in Figs. 17 and 18 was compared with the previous
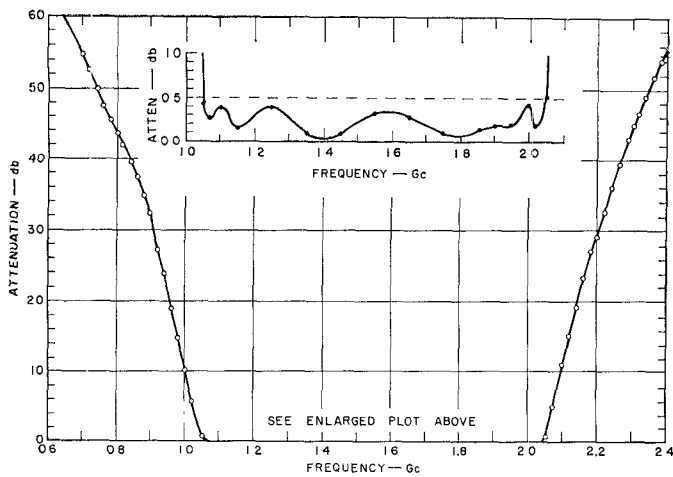
Fig. 15—Measured attenuation characteristic
of the filter in Fig. 13.

Fig. 17—A parallel-coupled strip-line filter with $\lambda_0/2$ resonators.

Fig. 16—Measured VSWR of the filter in Fig. 13.

Fig. 18—An interdigital filter formed from the filter in Fig. 17 (each $\lambda_0/2$ resonator has been cut in two in the middle and then folded double).

TABLE VII

COMPARISON OF THE MEASURED ATTENUATION IN FIG. 15
WITH ATTENUATION PREDICTED AS IN FIG. 4

(Computed values are for 0.10-db ripple, $n = 8$,
$w = 0.645$, and $f_0 = \omega_0/(2\pi) = 1.55$ Gc)

f, Gc	L_A, db for $L_{Ar} = 0.10$	L_A, db Measured
0.90	32	31
2.23	32	33
0.70	56	55
2.43	56	57

(a)

(b)

Fig. 19—Effect of folding a $\lambda_0/2$ resonator
to make a $\lambda_0/4$ resonator.

interdigital-line exact analysis[4] for the case where there is no fringing beyond nearest neighbors. Surprisingly enough, the image bandwidths were practically the same (to slide rule accuracy) by either theory, even for bandwidths as great as an octave. This unexpected result indicates that the folding process in Fig. 18 should not greatly disturb the response of filters of the form in Fig. 17, even if the bandwidth is quite wide (provided that fringing capacitances beyond nearest-neighbor line elements are negligible). Experimental results show that in typical cases the fringing capacitance beyond nearest neighbor has no serious effect.

The equations in Table II were derived directly from the equations in Table I in Matthaei[6] in dual form (which apply to filters of the form in Fig. 17),[15] but with two generalizations. First, the equations were generalized so that, if desired, they can be used with lumped-element prototypes that are neither symmetrical nor antimetrical (*i.e.*, one half of the network is not the reciprocal of the other half).[7] Second, they were generalized so that the admittance level within the filter can be adjusted as desired. This last feature was made possible by adding an additional degree of freedom in the design of the end sections of the filter. In the procedure discussed in Matthaei[6] all of the parallel-coupled sections of the filter, including the end sections 0, 1 and n, $n+1$, have parallel strips with identical widths. By allowing the widths of the strips in the end sections to be unequal, an additional degree of freedom is obtained, which permits arbitrarily fixing the admittance level in the interior of the filter.

Fig. 20 shows a strip-line parallel-coupled section with short circuits, and its exact equivalent in open-wire line.[16] It is interesting to note that the capacitances C_a and C_b per unit length between the strip-lines and ground become the capacitances per unit length of the short-circuited open-wire stubs. The capacitance C_{ab} per unit length between strip-lines becomes the capacitance per unit length of the open-wire connecting line. By use of this equivalence, the filter in Fig. 17 can be converted to an exactly equivalen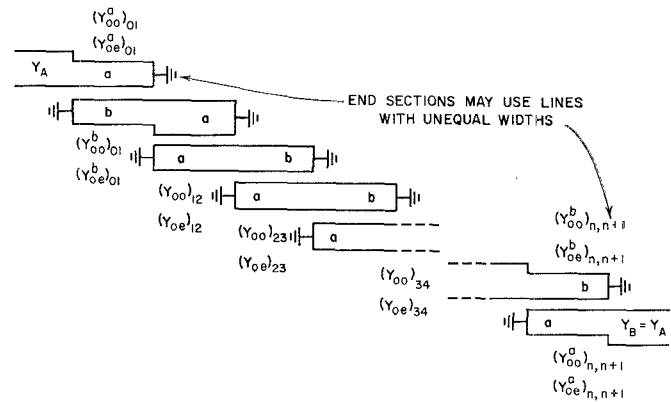t filter consisting of shunt stubs with connecting lines.[6] If the constraint $Y_{oe}{}^a + Y_{oo}{}^a = 2Y_A$ is enforced in the design of the end sections, the open-wire equivalent circuit in Fig. 20 reduces exactly to the remarkably simple circuit shown on the right in Fig. 21. The admittance scale factor h in Table II is exactly

$$h = \frac{1}{N^2} \tag{12}$$

where N is the turns ratio of the ideal transformer in Fig. 21. The admitttance scale factor h used in Table II corresponds to s/Y_A in the equations in Table I in Matthaei in dual form.[18] In Matthaei,[6] the scale factor s was so specified as to make the widths of the end strips equal, while in the derivation of the equations herein, $h = s/Y_A$ is arbitrary.

When generalized design equations had been prepared for the filter circuit in Fig. 17, the design equations in

Fig. 20—Short-circuited, parallel-coupled strip-lines and their open-wire-line equivalent circuit (the parallel-coupled lines may be of either equal or unequal widths).

Fig. 21—Special properties of the circuits in Fig. 20 when a special constraint is applied.

Table II were obtained directly by use of the "folding" approximation in Fig. 18. Since the equations for the filter in Fig. 17 were shown to be valid from narrow bandwidths to at least bandwidths of the order of an octave, and since the folding approximation appears to be reasonably good to such bandwidths, the design equations in Table II should, in principle, be good for large as well as for narrow bandwidths. However, the physical dimensions of the wide-band structure are not as desirable as those of the filters shown in Fig. 2.

In order to derive design equations for interdigital filters with open-circuited terminating lines (Fig. 2), design equations were first derived for the type of filter shown in Fig. 22. This filter is nearly the same as the parallel-coupled filter in Fig. 17, except for the manner in which the terminating lines are coupled in. It is readily seen that if the folding process in Fig. 18 is applied to the filter in Fig. 22, an interdigital filter with open-circuited input lines will result. It might seem at first that design equations for interdigital filters with open-circuited terminating lines could have been obtained by folding a parallel-coupled filter that had resonators open-circuited at the ends.[5,6] However, it will be seen that this cannot work, since the voltages at opposite ends of a $\lambda/2$ resonator have opposite polarity.

[15] The equations in Table I in Matthaei[6] are for filters with parallel-coupled resonators with open-circuited ends. Equations for the filter in Fig. 17 were obtained by duality, as is discussed in Matthaei.[6]

[16] The equivalences shown in Figs. 20, 21, and 23 were derived by extension of the work of Jones and Bolljahn,[11] and of Ozaki and Ishii.[17]

[17] Hiroshi Ozaki and Junya Ishii, "Synthesis of a class of strip-line filters," IRE TRANS. ON CIRCUIT THEORY, vol. CT-5, pp. 104–109; June, 1958.

[18] The parameter s in Table I in Matthaei[6] has the dimensions of ohms. In the dual equations, which apply to the circuit in Fig. 17. s has the dimensions of mhos and s/Y_A is dimensionless.
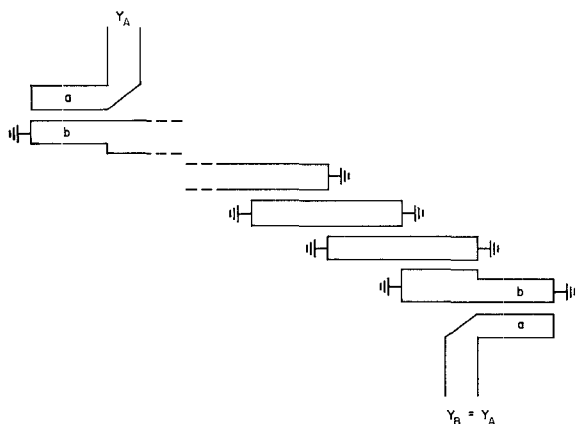
Fig. 22—A parallel-coupled filter with $\lambda_0/2$ short-circuited resonators and open-circuited terminating lines.
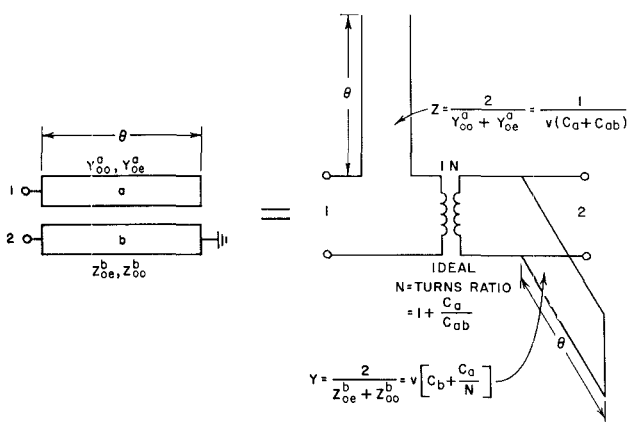

Fig. 23—An additional parallel-coupled strip-line section and its open-wire-line equivalent circuit.
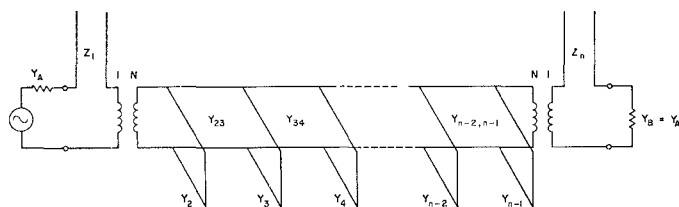

Fig. 24—An open-wire-line equivalent circuit of the filter in Fig. 22 (all stubs and connecting lines are $\lambda_0/4$ long at midband).

Design equations for the filter in Fig. 22 were derived in a manner much like that used for deriving the equations for the filter in Fig. 17, except that the parallel-coupled information summarized in Fig. 23 was used in designing the end sections. Note that this section also has impedance transforming properties [(12) applies], and that the open-wire equivalent circuit in this case has both a series and a shunt stub. In the case of Fig. 21, the constraint equation applied causes one natural mode of vibration to be stifled, and as a result the equivalent circuit has only one stub. Using the end section in Fig. 23, all of the natural modes of vibration of the circuit are fully utilized.

When the strip-line and open-wire line equivalences in

Figs. 20 and 23 are used, it will be seen that the strip-line circuit in Fig. 22 is electrically identical to the open-wire line circuit in Fig. 24. The filter circuit in Fig. 24 is very similar to the filter in Fig. 3 in Matthaei,[6] for which design equations were presented in Table III in Matthaei.[6] The filters in Fig. 24 and in Fig. 3 in Matthaei[6] become identical if we set $a = \infty$ for Fig. 3 and if we introduce an ideal transformer at each end of the filter and alter the impedance level within the filter to make the over-all performance the same as before the transformers were introduced. Design equations for the filter in Fig. 24 were obtained in this manner, and also equations for the equivalent filter in Fig. 22.[19] Then the equations for the corresponding interdigital filter were obtained by applying to the filter in Fig. 22 the folding approximation illustrated in Fig. 18. The reader will be interested to note that the $J_{k,k+1}$ in Table V correspond to characteristic admittances $Y_{k,k+1}$ of the connecting lines in Fig. 24, while Z_1, Y_2, Y_3, $\cdots$, Y_{n-1}, Z_n in Table V correspond to the characteristic impedances or admittances of the stubs in Fig. 24, for the limiting case where the transformer turns ratio is $N = 1$. For $N > 1$ the admittances are scaled by the factor h.

VII. Conclusions

The approximate equations developed for the design of interdigital band-pass filters were found to yield reasonably accurate results when used for design of either narrow- or wide-band band-pass filters. By making allowance for about a 7 per cent shrinkage in fractional bandwidth as compared to the value inserted in the equations, and by providing for small adjustment in the gap spacing at each end of the filter, desired performance should be obtainable with high accuracy. The design equations are simple to use, and the trial designs performed very much as expected. The trial designs demonstrated that practical interdigital filters can have the attractive features that were anticipated: they can be made very compact; the relatively large spacings between their resonator elements permit relatively relaxed tolerances; they have strong stop bands with the second pass band at three times the frequency of the first pass band; they make spurious response impossible at or near twice the first pass-band frequency; and they can be fabricated using little or no dielectric material.

[19] The design equations in Matthaei[6] were in this present work also modified to include the situation where the low-pass prototype might not be either symmetrical nor antimetrical.